Bifunctional Nano Lycurgus Cup Array Plasmonic Sensor for Colorimetric Sensing and Surface-Enhanced Raman Spectroscopy

Te-Wei Chang, Xinhao Wang, Austin Hsiao, Zhida Xu, Guohong Lin, Manas Ranjan Gartia, Xiangrong Liu,* and Gang Logan Liu**

A bifunctional ultrasensitive nanoplasmonic sensor is demonstrated with combined surface plasmon resonance (SPR) and surface-enhanced Raman spectroscopy (SERS) sensing capabilities. Unlike traditional extraordinary transmission (EOT) devices, nano Lycurgus cup array (nanoLCA) contains a hybrid configuration of periodic quasi-3D nanostructure array and dense sidewall metal nanoparticles within each nanostructure, which enables both refractive index sensing and SERS chemical identification on the same device with high sensitivity. The visible plasmon resonance sensitivity of nanoLCA is measured to be as high as 796 nm/RIU with the figure of merit (FOM) of 12.7 so that the device is applied for colorimetric liquid sensing with an ordinary microscopic system. Moreover, the SERS enhancement of the very same nanoLCA for liquid sample is calculated to be 2.8×10^7, which is the highest among all reported EOT-based SERS devices. The urea concentration detection has been demonstrated to show the complementary rapid colorimetric screening and precise SERS identification functions provided by nanoLCA plasmonic sensor for chemical analysis or biological diagnostics in a resource-limited environment.

1. Introduction

With the advance in nanofabrication technology, noble metallic nanostructure reveals its advantages on various applications including chemical and biological sensing, subwavelength imaging, power harvesting, and medical treatment.[1–4] The versatility is attributed to the unique plasmonic properties of metallic nanostructure, which lead to surface plasmon resonance (SPR) and localized surface plasmon resonance (LSPR).[5] Refractive index sensing is one of the important plasmonic applications, which provides an accurate and non-labeling analytical method. This technique is based on monitoring wavelength or angle shift of the resonance peak when the surrounding condition of metallic nanostructure is changed by replacing the bulk dielectric material or inducing molecular interaction on the nanostructure surface.[6] It has been implemented by several different configurations including Kretschmann configuration, subwavelength grating, nanoparticle-based sensor, and extraordinary transmission (EOT) device.[7,8] Refractometric sensing coupled with subwavelength grating reduces the size and complexity of prism integration of Kretschmann configuration. However, it loses the ultrahigh sensitivity achievable by Kretschmann configuration.[9] On the other hand, sensing technique based on LSPR mode in metal nanoparticles demands less instrumental requirement compared to SPR sensors. However, it suffers from low uniformity and reproducibility because the particle size and spatial distribution of metal nanoparticle are difficult to control precisely. Furthermore, the LSPR sensitivity is usually lower than SPR sensitivity.[10] Shen et al.[11] lately proposed an LSPR-based periodic gold mushroom array, which exhibits ultrahigh sensitivity and figure of merit (FOM) due to its WA-LSPR mode at infrared region. However, this device is not operated in visible range, which means that it cannot be simply applied on conventional optical spectroscopic system.

Recently, nano Lycurgus cup array (nanoLCA) plasmonic sensor has been demonstrated its advantages in refractive index sensing.[12] Unlike most of other EOT sensors, which are fabricated by expensive and time-consuming processes

Dr. T.-W. Chang, X. Wang, Dr. Z. Xu, G. Lin, Prof. G. L. Liu
Department of Electrical and Computer Engineering
Micro and Nanotechnology Laboratory
University of Illinois at Urbana Champaign
Urbana, IL 61801, USA
E-mail: loganliu@illinois.edu
Dr. A. Hsiao
Department of Bioengineering
University of Illinois at Urbana Champaign
Urbana, IL 61801, USA
Dr. M. R. Gartia
Department of Mechanical and Industrial Engineering
Louisiana State University
Baton Rouge, LA 70803, USA
E-mail: mgartia@lsu.edu
Prof. X. Liu
Department of Computer Science
XiamenUniversity
Xiamen 361005, Peoples R China
E-mail: loganliu@illinois.edu

DOI: 10.1002/adom.201500092

such as focus ion beam milling or electron beam lithography, the fabrication of nanoLCA is based on the large-area and cost-effective nanoreplica technique. Besides, the huge absolute peak wavelength shift from nanoLCA opens an opportunity for colorimetric sensing by simple microscopic system or naked eye instead of applying complicated spectroscopic system. Although nanoLCA has shown its significant advantages on plasmonic colorimetric sensing, its application is still limited by the nature of refractive index sensing technique: high purity of sensing environment is required and the probing molecule must be identified beforehand; otherwise the undesired interference from impurities may lead to false positive or readout error for quantitative measurement. Although the surface functionalization can increase the specificity to the targeted molecule, however, it requires specialized laboratory facilities and professional personnel to perform time-consuming and multi-steps procedures. As a result, it is not suitable in point-of-care or a resource-limited environment.

In contrast, Raman spectroscopy is able to precisely identify chemical molecules by their distinctive molecular vibrational modes. Moreover, surface-enhanced Raman spectroscopy (SERS) greatly extends this capability to ultralow concentration detection.[13] SERS has been performed on several devices, which have similar configuration as nanoLCA such as nanohole array and quasi-3D devices. However, the Raman enhancements of these devices are moderate (≈10^3 to 10^6) compared to other SERS substrates and difficult to meet the practical requirement of detection at lower analyte concentration.[14–17]

In this paper, we demonstrated the bifunctional property of nanoLCA, which possesses combined colorimetric sensing and SERS capability. Similar idea of multifunctional plasmonic sensor has been reported in other literatures; however, none of those devices has satisfactory performance with both refractive index sensing and SERS for practical applications.[18,19] The simulated and experimental results presented here show that the unique configuration of nanoLCA, which is a hybrid combination of a periodic quasi-3D nanostructure array pattern and dense sidewall metallic nanoparticles, enables both high sensitivity and sharp resonance peak in refractive sensing. Besides, we demonstrated the highest Raman enhancement from nanoLCA device compared with any other reported periodic EOT-based devices in a liquid-sensing environment. This dual functionality of nanoLCA shows great potential to provide a sensing platform, which can rapidly screen large amount of liquid samples by colorimetric sensing with minimum sample preparation and facility requirement. Subsequently, the capability of SERS from the same device is able to perform molecule identification on selected samples. It compensates the deficiency of both low specificity on refractive index sensing and nonlinearity on SERS molecule quantification.

2. Results and Discussion

2.1. Nanofabrication of NanoLCA Plasmonic Sensors

The schematic of nanoLCA fabrication process is shown in **Figure 1**a. First, a nanocone glass master mold was prepared by the laser interference lithography technique. Then the pattern was transferred to an optically transparent flexible polyethylene terephthalate (PET) film by the UV-curing nanoreplica process. Finally thin layers of 9 nm titanium (Ti) and 90 nm silver (Ag) were deposited on the replicated device by the electron beam evaporation. Ti was used as an adhesive layer to tightly bond Ag to the polymer substrate. The images of scanning electron microscopy (SEM) are shown in Figure 1b,c. It can be clearly observed that nanoLCA holds high uniformity after the replication process and each nanocup contains a top Ag layer and bottom Ag nanodisk, which is similar to quasi-3D device.[15] Moreover, due to the unique cup-shaped profile of nano Lycurgus cup, a dense array of sub 50 nm Ag nanoparticles was formed on the sidewall after metal deposition.

2.2. Optical Characterization

In order to understand the plasmonic property of nanoLCA device, 3D-finite-difference time-domain (FDTD) method was applied to simulate the optical characterization based on this

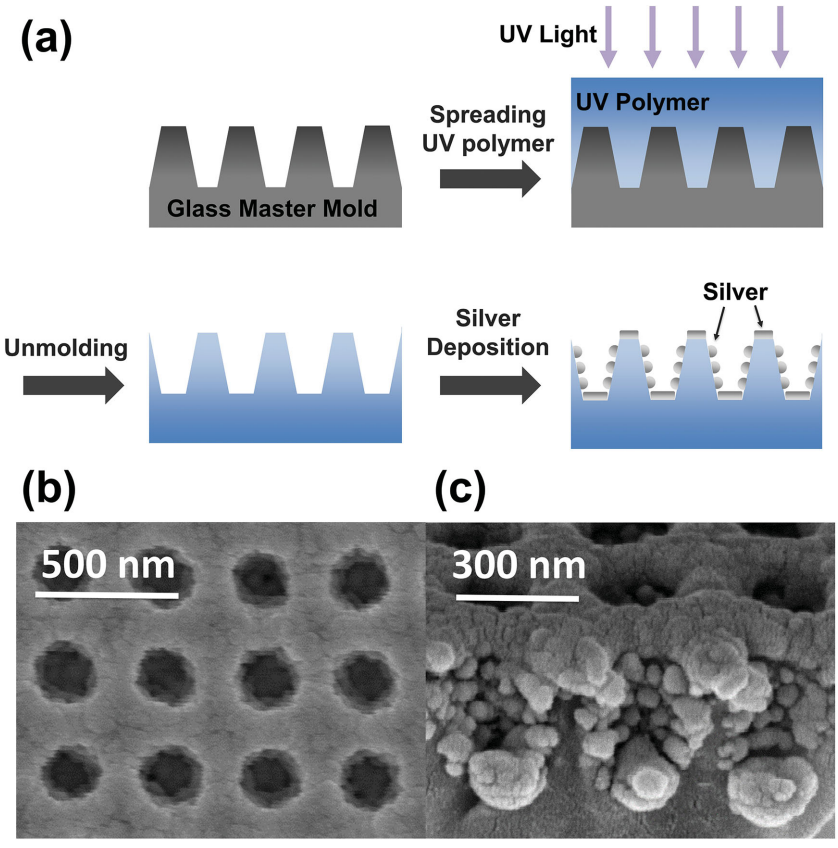

Figure 1. a) Schematic of nanoLCA plasmonic sensor fabrication; b) top side and c) 60° tilted angle view SEM images of nanoLCA plasmonic sensor fabrication.

configuration. First Ag plane thin film, single and periodic cup-shaped nanostructure (profile is the same as nano Lycurgus cup) with only top Ag layer were compared to identify the resonance peaks. The thickness of a top Ag layer in all the geometries was kept the same as 90 nm. Figure S1 (Supporting Information) shows the transmission spectra of all three configurations and the cross-section *z*-direction electric field (E_z) distribution of periodic cup-shaped nanostructure with a top Ag layer at the wavelength of 354, 455, and 644 nm. All three transmission spectra exhibit resonance peak at 320 nm, which is related to bulk plasma of Ag.[20] Additional peak at 354 nm appears in both single and periodic nanostructures. According to the electric field distribution at 354 nm, the strong electric field is focused on the upper rim edge of the top Ag layer, which indicates that this peak is due to LSPR.[21] On the other hand, peaks at 455 and 644 nm are only found in the periodic case. Moreover, the cross-section electric field at both wavelengths is focused at the interface of air–Ag and Ag–substrate, which is the signature pattern of SPR mode.[22] Therefore, these two peaks can be identified as surface plasmon polariton-Bloch wave (SPP-BW) modes.[23–25] Peaks at 455 and 644 nm are related to (1,0) mode at air–Ag and Ag–substrate interface, respectively. Other literature has also identified these two modes at similar wavelengths for the periodic nanostructured device with the same periodicity.[26]

Based on the previous analysis, the resonance peaks from a cup-shaped nanostructure array with a top Ag layer are identified. However, comparing to the actual nanoLCA configuration, some important structural components of nanoLCA such as the bottom Ag nanodisk and sidewall Ag nanoparticles are not included yet. Hence, a step-by-step analysis of adding these components was performed to understand the unique configuration of nanoLCA and its resonance conditions. The study will elucidate the mechanism of nanoLCA resonance compared to other EOT devices. The simulation model of nanoLCA was based on the observation of SEM images and shown in **Figure 2**a. Since in reality the sidewall Ag nanoparticles are randomly distributed, different diameter (*D*) of sidewall Ag nanoparticle (*D* = 30, 40, and 50 nm) were simulated to match the measurement data as shown in Figure 2b. We modeled the sidewall Ag nanoparticles to be in four rows and evenly distributed in height. In each row, there were eight nanoparticles as observed in the SEM images. From the simulation results, Ag nanoparticles with the diameter of 40 nm on the sidewall matched the experimental data the best and were applied in the following analysis.

Figure 2c depicts the transmission spectra through the same periodic cup-shaped nanostructure but with different Ag components. Spectrum A, B, C, and E are simulated transmission spectra with a top Ag layer, bottom Ag nanodisk, quasi-3D configuration (refers to the combination of a top Ag layer and bottom Ag nanodisk), and nanoLCA configuration, respectively. The scattering spectrum of only sidewall Ag nanoparticles is also included in the figure as spectrum D. It can be observed that the resonance peaks from top Ag layer only (spectrum A) and bottom Ag nanodisk only (spectrum B) are coupled to form multiple resonance peaks at 438, 463, and 495 nm in quasi-3D configuration (spectrum C). This phenomenon of coupled resonance was observed in other literatures as well.[27,28] However, when the sidewall Ag nanoparticles are taken into consideration, the scattering from sidewall Ag nanoparticles (spectrum D)

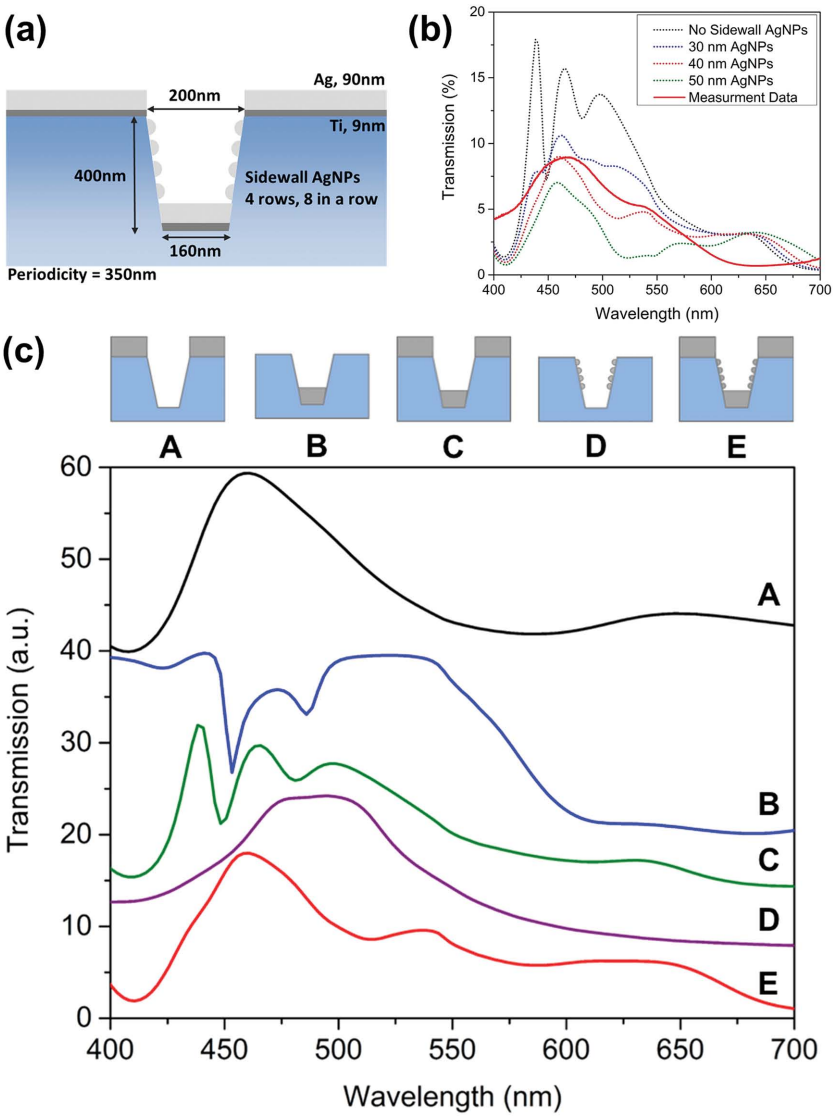

Figure 2. a) Simulation model of nanoLCA plasmonic sensor; b) Simulated transmission spectra of nanoLCA with no sidewall Ag nanoparticles and different sizes of sidewall Ag nanoparticles (diameter = 30, 40, and 50 nm). The measured transmission spectrum of nanoLCA is shown in the figure as well for comparison; c) Simulated transmission spectra of periodic cup-shaped nanostructure with (A) top Ag layer; B) bottom Ag nanodisk; C) quasi-3D configuration; E) actual configuration of nanoLCA. Scattering spectrum of only sidewall Ag nanoparticles is plotted in the figure as well as spectrum D.

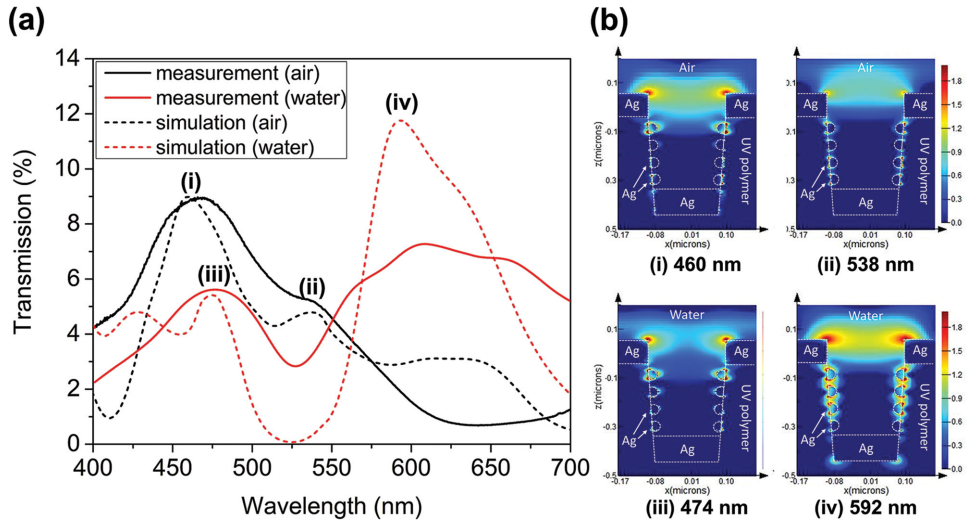

Figure 3. a) Comparison of simulated and measured transmission spectra of nanoLCA covered with air and water; b) The logarithm electric field intensity of nanoLCA at 460 and 538 nm with air (i and ii) and 474 and 592 nm with water (iii and iv) (enlarged figure can be found in Figure S4, Supporting Information).

is in the same spectral range as coupled resonance peaks of quasi-3D configuration. As a result, a single and sharper resonance peak with full-wave half maximum (FWHM) of ≈50 nm comparing to traditional nanohole array configuration (refers to spectrum A in the figure with FWHM of ≈100 nm) is formed and plotted in spectrum E. This sharper FWHM is beneficial for refractive index sensing providing better FOM as well as in the image analysis of colorimetric sensing.

The comparison of transmission spectra between simulated and experimental data is shown in **Figure 3**a. Air (n = 1) and water (n = 1.333) superstrates, which were defined as the dielectric material above the nanoLCA device, were examined and presented in the figure. The logarithm electric field intensity of corresponding resonance peaks is shown in Figure 3b. In general, the simulated model predicts the actual optical phenomenon very well despite minor resonance offsets at longer wavelength with water superstrate (610 nm in experiment and 592 nm in simulation). From the electric field intensity diagrams, it can be found that peaks (i) and (iii) are in the same resonance mode in different superstrates, where the electric field is mainly focused at the upper edge of the top Ag layer and the first row of sidewall Ag nanoparticles. On the other hand, peaks (ii) and (iv) are in the same resonance condition since the electric field patterns are the same and have strong coupling among sidewall Ag nanoparticles. It can also explain the minor resonance offset at longer wavelength with water superstrate mentioned before: the difference between the simulated and measured spectra of the nanoLCA may be due to the limitations in the simulation software to accurately represent the quasi-random spatial distribution of sidewall Ag nanoparticles.

2.3. Characterization of Colorimetric Sensing Performance

To characterize the colorimetric sensing performance of nanoLCA, glycerol solutions with different wt% concentrations (0%, 3%, 10%, 20%, 30%, and 40%) were used to vary the refractive index of superstrate covered on nanoLCA. The measured results of transmission spectra are shown in **Figure 4**a. It can be observed that the resonance peaks were red-shifted when the refractive index of superstrate increased. 3D-FDTD simulation with the same condition is shown in Figure 4b. From the simulation, the wavelength shift of resonance peaks is consistent with the measurement results. Figure 4c depicts the peak resonance shift with respect to the refractive index change of superstrate by analyzing the resonance peak at shorter wavelength (refer to the peak at 465 nm with 0% concentration of glycerol). The sensitivity ($\Delta\lambda/\Delta n$, λ is the wavelength and n is the refractive index) was calculated to be 796 nm/RIU by using the linear curve-fitting method. The maximum figure of merit (FOM = sensitivity/Δw, where Δw is the FWHM of the peak inconsideration) is calculated as 12.7 with the FWHM width of 62.55 nm at that resonance peak. The corresponding bright-field optical images of the spectral measurement are shown in Figure 4d and demonstrate the colorimetric sensing capability of nanoLCA with simple microscope setup. As the concentration of glycerol increased, the color of transmission optical image became more reddish, which is consistent with the red-shifting phenomenon in the experimental transmission spectrum results.

2.4. Characterization of SERS Performance

The SERS capability of nanoLCA device was analyzed by applying monolayer of 1,2-bis(4-pyridyl)ethylene (BPE, 99%; Sigma–Aldrich) as the probing molecule. First the nanoLCA devices were immersed in 5×10^{-3} M BPE ethanolic solution for 24 h and then rinsed with pure ethanol solution in order to wash out extra BPE molecules stacked on the surface. Finally devices were blown with nitrogen gas to completely dry. **Figure 5**a shows the extinction spectra of nanoLCA device with air and water superstrates. It can be observed that nanoLCA exhibits higher absorption at 633 nm in water than in air, which

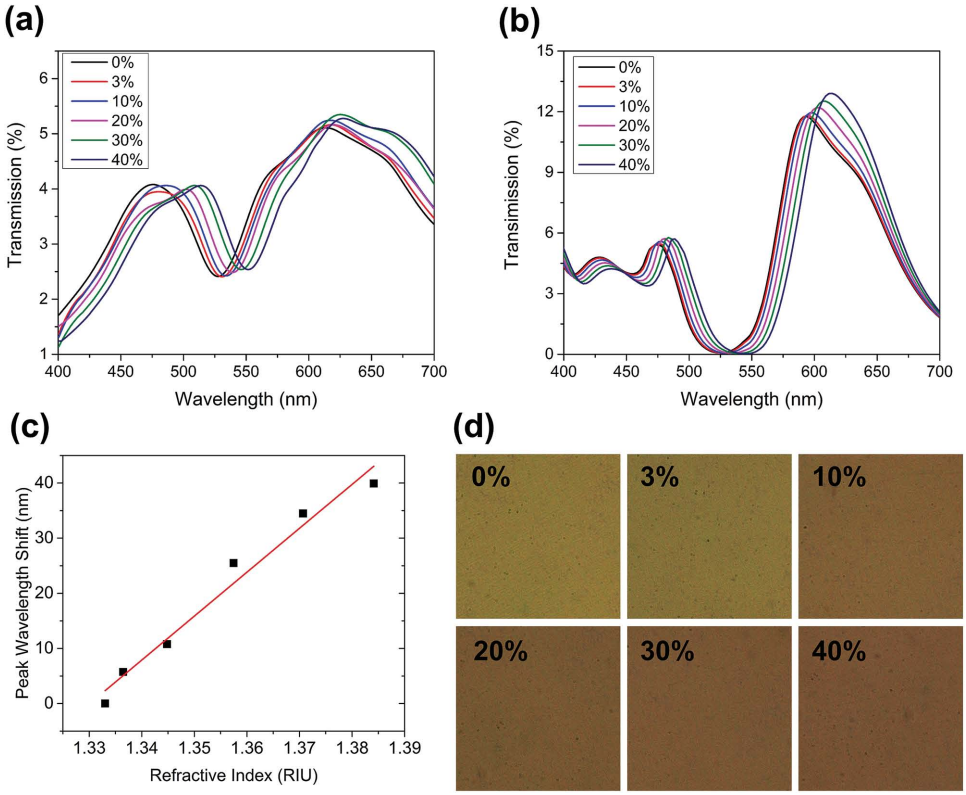

Figure 4. a) Measured and b) simulated transmission spectra of nanoLCA covered with different wt% concentrations of glycerol (0%, 3%, 10%, 20%, 30%, and 40%); c) Sensitivity of nanoLCA calculated for glycerol concentration range from 0% to 40%. The sensitivity was calculated as 796 nm/RIU; d) Optical images of different wt% concentrations of glycerol on nanoLCA.

indicates the resonance should be stronger in water with the excitation wavelength at 633 nm. As shown in Figure 5b, the simulated logarithm electric field intensity with water superstrate also possesses much stronger near field than the case in air especially among the sidewall Ag nanoparticles. The simulated results further proved that nanoLCA device is optimized for liquid SERS detection with 633 nm excitation wavelength. Figure 5c shows the Raman spectra of BPE on nanoLCA in both air and water. For comparison, commercially available Klarite SERS substrate (Klarite KLA-313, D3 Technologies Ltd., UK) was measured with the same treatment and the result is included in the figure as well. All spectra show characteristic Raman peaks of BPE at 1020, 1200, 1340, 1607, and 1637 cm^{-1}. It can be observed that the Raman enhancement is approximately 20 times higher when nanoLCA covered with water than air after normalization of excitation laser power, which matches the trend that nanoLCA exhibits higher resonance with water superstrate from the results of extinction spectra and FDTD simulation. Furthermore, nanoLCA device under solution-based detection environment provides 148 and 107 times better performance than the commercial available Klarite SERS substrate with air and water as superstrate. The minor Raman signal improvement of Klarite SERS substrate in water compared to air can be attributed to the low-resonance peak shift respect to refractive index change.[29] The enhancement factor (EF) is estimated by the integration of peak intensity at 1607 cm^{-1} with respect to the bulk BPE solution and calculated to be 2.8×10^7. (The detail information of EF calculation can be found in Supporting Information.) This is so far the highest SERS enhancement achieved compared to other EOT devices such as nanohole array or quais-3D devices (The list of SERS performance from other similar EOT devices can be found in Supporting Information). In addition, most of the SERS performance from other devices were characterized and optimized under dry-state measurement; however, most of the chemical or biological molecules are existed in a solution-based environment. Therefore, the actual SERS performance from those devices might be lower with the application of solution-based measurement. The nanoLCA device shows its great advantage for in vivo SERS detection or rapid SERS testing with minimal sample preparation time (no waiting time to dry the sample), at the same time, it possesses comparable sensitivity in refractive index sensing compared to other types of plasmonic sensor. To examine the uniformity of SERS performance of nanoLCA device, a mapping of SERS spectra on nanoLCA was performed and the peak intensity at 1607 cm^{-1} is shown in Figure 5d. The total mapping is carried out on an area of 1 mm × 1 mm and measured at a spacing of 100 μm. The averaged intensity of total measured data was set as baseline (0% in the figure) to estimate the uniformity of spatial SERS performance. The relative standard deviation (RSD) was calculated as 10.2%, which demonstrates the high spatial uniformity of nanoLCA device in SERS detection for quantitative measurement.

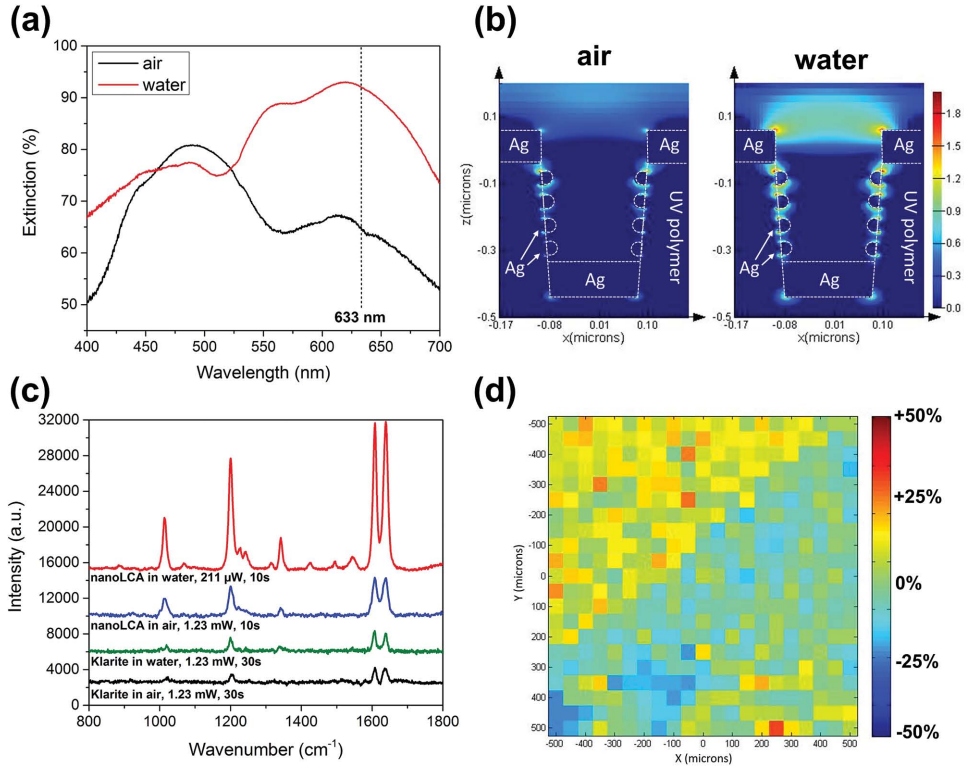

Figure 5. a) Extinction spectra of nanoLCA covered with air and water; b) The logarithm electric field intensity of nanoLCA with superstrates of air and water (enlarged figure can be found in Figure S4, Supporting Information); c) Raman spectra of BPE on both nanoLCA and commercially available Klarite SERS substrate covered with air and water; d) Mapping of Raman intensity at 1607 cm^{-1} of BPE on nanoLCA at excitation wavelength 633 nm. The total mapping is on area of 1 mm × 1 mm and measured at every 100 μm distance.

2.5. Detection of Urea Concentration

In this section, the detection of urea concentration was demonstrated as a proof-of-concept to show the potential of utilizing the dual functionality of nanoLCA for diagnostics under resource limited environment: on-site plasmonic colorimetric screening can be performed with ordinary bright-field microscopy to rapidly select out the samples of interest (without specificity). This sample-screening process requires minimum laboratory facility, sample preparation, and professional personnel. Later on the selected samples can be further analyzed for identification of the molecules with high specificity by Raman spectroscopy with the same nanoLCA plasmonic device. This complementary two-step analytical procedure provides a sensing platform with high speed, sensitivity, and specificity while minimizing probability of false positive.

Urea is one of the major components in urine and plays a significant role in maintaining fluid and electrolyte balance in the body.[30] Urea concentration in urine is directly related to the amount of protein intake. Sudden decrease of urea concentration indicates the protein breakdown, which is the hint of acute kidney failure, malnutrition, and severe liver damage. **Figure 6** demonstrates the results of both colorimetric and Raman spectroscopy detection of urea concentration by nanoLCA plasmonic device. Ordinary bright-field microscopy (with filters) was used to take optical images with different concentrations of urea solution (0×10^{-3}, 25×10^{-3}, 50×10^{-3}, 100×10^{-3}, 250×10^{-3}, 500×10^{-3}, 750×10^{-3}, and 1000×10^{-3} M). All the images were taken with FITC emission filter, which only allows the light between 505 to 535 nm to be captured by the CCD camera. This step is able to avoid the interference from

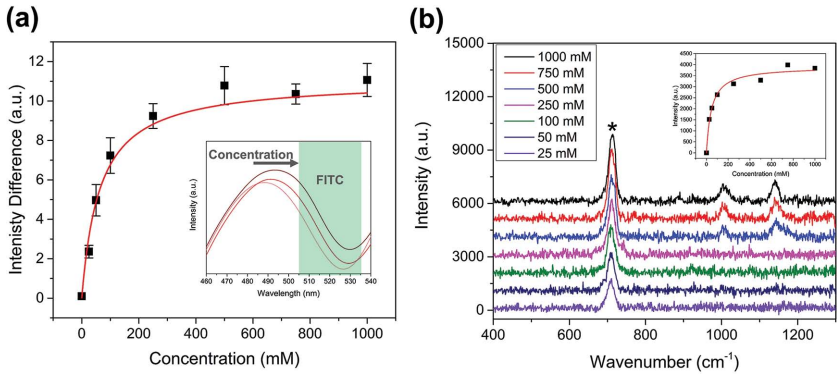

Figure 6. a) Averaged green-channel intensity of nanoLCA device with different concentrations of urea. All images are taken with FITC filter applied. The inset figure demonstrates the shift of transmission spectrum when the concentration of urea becomes higher (25×10^{-3} to 100×10^{-3} M in this example). The green shadow region represents as the filtered band of FITC in spectrum; b) Raman spectra of nanoLCA device with different concentrations of urea at 708 cm^{-1}.

incident light within other wavelengths. As shown in the inset of Figure 6a, when the urea concentration increases, the resonance peak experienced red shift due to the increase of refractive index. As a result, the total intensity within FITC-filtered range will be increased accordingly. Figure 6a shows the averaged green-channel intensity extracted from images with respect to urea concentration. The relationship curve fits to the Langmuir equation since urea has strong adsorption to the silver surface.[31] The peak wavelength shift of different urea concentrations measured by spectrometer shows consistence to the intensity based colorimetric measurement (see Supporting Information). The results of Raman spectroscopy are shown in Figure 6b with the same concentrations of urea as used in the colorimetric measurements. All spectra show the dominant peak at 708 cm^{-1}, which is π_{CO} vibrational mode when the urea is adsorbed on the silver surface. With the concentration higher than 500×10^{-3} M, peaks at 1007 and 1145 cm^{-1} can be observed, which are related to Raman peaks from bulk urea molecules.[32] The plot of peak intensity at 708 cm^{-1} with respect to different concentrations of urea is shown in the inset of Figure 6b. The intensity curve is also fit to the Langmuir equation and further validates the results obtained from colorimetric measurement. This experiment proves the concept of utilizing the capability of molecule identification from SERS to increase the specificity to the refractive index sensing, while the colorimetric screening process can quickly recognize the targeted sample with minimum sample preparation. Most of all, these two sensing methods can be directly performed on the very same device without any modification.

3. Conclusion

In summary, bifunctional nanoLCA plasmonic device has been developed and demonstrated for both colorimetric and SERS sensing. Proved by both simulation and experiments, the unique configuration of nanoLCA, which contains periodic quasi-3D nanostructure and dense Ag sidewall nanoparticles, leads to sharper FWHM (≈50 nm) compared to traditional nanohole array device (≈100 nm). The sensitivity was calculated as 796 nm/RIU with the FOM of 12.7 and the capability of utilizing nanoLCA for colorimetric sensing has been performed as well. In addition, the Ag sidewall nanoparticles contribute to strong coupling and enable the nanoLCA device to be optimized for SERS measurement under the solution-based environment, where most of the biological and chemical analyses are typically performed. The SERS EF was calculated as 2.8×10^7 under a solution-based environment with 10.2% RSD, which is so far the highest reported SERS enhancement achieved with similar periodic EOT devices. Finally, the detection of urea concentration has been demonstrated as proof-of-concept of a two-step sensing process, which enables rapid on-site screening and further molecule identification.

4. Experimental Section

Fabrication of nanoLCA: The glass master mold is consisted of nanocone array, which is fabricated by the laser interference lithography technique.[33] The periodicity, height, and width of nanostructure are 350, 500, and 200 nm. Before nanoreplica process, the glass master mold was immersed into dimethyl dichlorosilane solution for 30 min. The mold was rinsed with DI water and ethanol to wash out extra molecules to form a monolayer saline on the mold surface. This step is to achieve hydrophobic surface for the master mold and be able to assist in the removal of cured polymer replica. About 10 μL UV-curable polymer (NOA-61) was evenly spread on the nanopillar surface. A 250 μm thick flexible PET sheet was used as a supporting substrate for replica process. UV light-curing flood lamp system (Dymax EC-Series) was applied for providing constant UV light with power density of 105 mW cm^{-2}. The curing time was set as 60 s. After replication, metal deposition was implemented by the CHA SEC-600 e-beam evaporator system. The power of electron beam was set at 10 kV and operating base pressure was around 10^{-7} Torr. The deposition rate was controlled at 1 Å s^{-1} to ensure surface uniformity.

FDTD Simulation: The numerical simulations of optical characteristic were studied by using the 3D-FDTD method with FDTD software package from Lumerical Solutions, Inc. The *x*-axis-polarized electromagnetic wave was set to propagate normal to the substrate (-*z*-direction) for reflection, transmission, and near-field simulations. Perfect matching layer (PML) was applied to the boundary conditions in *z*-axis to eliminate any interference from the boundaries. In addition, PML aperiodic boundary was applied at *x*- and *y*-axes for simulating single and array nanostructure, respectively. The near-field simulation observed in this paper is at *x*–*z* plane where $y = 0$. The mesh size was set as 1.5 nm and the total FDTD simulation region was 350 nm × 350 nm × 1000 nm.

Optical Characteristic: The optical images were collected by Olympus BX51 Upright Fluorescence Microscope equipped with mercury lamp in Micro and Nanotechnology Laboratory, University of Illinois at Urbana-Champaign. The microscope was set at bright-field mode without applying any filter. The light was focused onto the sample with 20× (NA = 0.45) objective lens. The transmission and reflection spectra were collected by the same microscopy setup with USB2000+ Fiber Optic Spectrometer by Ocean Optics. The detection wavelength range is from 200 to 1100 nm and the spectral resolution is up to 0.3 nm FWHM. The extinction spectrum shown here is defined as the subtraction from the measured transmission and reflection spectrum.

Raman Spectroscopy Measurement: Renishaw PL/Raman microspectroscope system was applied in this for SERS signal measurements. 633 nm He–Ne lasers are used as excitation light source. 20× objective lens (NA = 0.45) was used to focus/collect incident light and Raman signal onto/from the surface of nanoLCA plasmonic sensor. The range of collected wavenumber was from 200 to 2000 cm^{-1}. The acquisition time for nanoLCA plasmonic device and Klarite SERS substrate is 10 and 30 s. Every spectrum shown in this paper is the average value measured from five different spots.

Image Analysis: The filtered color images of nanoLCA device were taken by the same microscope system mentioned in optical characterization section at 20× magnification with exposure time of 50 ms (gain = 1; gamma = 1). FITC fluorescence emission filter was applied, which enables a narrow passing wavelength band from 505 to 535 nm. Each image contains three 8-bits channels of red, green, and blue. The image analysis was done by ImageJ software. For the calculation, an area of 512 × 512 pixels was selected to remove the boundary area.

Supporting Information

Supporting Information is available from the Wiley Online Library or from the author.

Acknowledgements

This work is supported bythe US Department of Energy under Grants DE-FG02-07ER46453 and DE-FG02-07ER46471. Prof. X. Liu's work

as avisiting scholar in the Micro and Nanotechnology Laboratory at University of Illinois was supported by National Natural Science Foundation of China (Grant Nos. 61472333).

Received: February 10, 2015
Revised: March 18, 2015
Published online: July 21, 2015

[1] T. Chang, M. R. Gartia, S. Seo, A. Hsiao, G. L. Liu, *Nanotechnology* **2014**, *25*, 145304.
[2] J. Li, M. Gu, *Biomaterials* **2010**, *31*, 9492.
[3] F. Chen, J. Wu, C. Lee, Y. Hong, C. Kuo, M. H. Huang, *Appl. Phys. Lett.* **2009**, *95*, 013305.
[4] X. H. Huang, I. H. El-Sayed, W. Qian, M. A. El-Sayed, *J. Am. Chem. Soc.* **2006**, *128*, 2115.
[5] N. C. Lindquist, P. Nagpal, K. M. McPeak, D. J. Norris, S. Oh, *Rep. Prog. Phys.* **2012**, *75*, 036501.
[6] A. J. Haes, R. P. Van Duyne, *Anal. Bioanal. Chem.* **2004**, *379*, 920.
[7] T. Chung, S. Lee, E. Y. Song, H. Chun, B. Lee, *Sensors* **2011**, *11*, 10907.
[8] S. Roh, T. Chung, B. Lee, *Langmuir* **2011**, *11*, 1565.
[9] L. S. Jung, C. T. Campbell, T. M. Chinowsky, M. N. Mar, S. S. Yee, *Langmuir* **1998**, *14*, 5636.
[10] S. J. Zalyubovskiy, M. Bogdanova, A. Deinega, Y. Lozovik, A. D. Pris, K. H. An, W. P. Hall, R. A. Potyrailo, *J. Opt. Soc. Am. A. Opt. Image Sci. Vis.* **2012**, *29*, 994.
[11] Y. Shen, J. Zhou, T. Liu, Y. Tao, R. Jiang, M. Liu, G. Xiao, J. Zhu, Z. Zhou, X. Wang, C. Jin, J. Wang, *Nat. Commun.* **2013**, *4*, 2381.
[12] M. R. Gartia, A. Hsiao, A. Pokhriyal, S. Seo, G. Kulsharova, B. T. Cunningham, T. C. Bond, G. L. Liu, *Adv. Opt. Mater.* **2013**, *1*, 68.
[13] K. A. Willets, R. P. Van Duyne, *Annu. Rev. Phys. Chem.* **2007**, *58*, 267.
[14] S. H. Lee, K. C. Bantz, N. C. Lindquist, S. Oh, C. L. Haynes, *Langmuir* **2009**, *25*, 13685.
[15] Q. Yu, S. Braswell, B. Christin, J. Xu, P. M. Wallace, H. Gong, D. Kaminsky, *Nanotechnology* **2010**, *21*, 355301.
[16] C. Ho, K. Zhao, T. Lee, *Nanoscale* **2014**, *6*, 8606.
[17] D. Wang, X. Yu, Q. Yu, *Nanotechnology* **2012**, *23*, 405201.
[18] V. Canpean, S. Astilean, *Lab Chip* **2009**, *9*, 3574.
[19] M. Potara, A. Gabudean, S. Astilean, *J. Mater. Chem.* **2011**, *21*, 3625.
[20] P. Chaturvedi, K. H. Hsu, A. Kumar, K. H. Fung, J. C. Mabon, N. X. Fang, *ACS Nano* **2009**, *3*, 2965.
[21] W. Yue, Y. Yang, Z. Wang, J. Han, A. Syed, L. Chen, K. Wong, X. Wang, *J. Phys. D: Appl. Phys.* **2012**, *45*, 425401.
[22] L. Salomon, F. Grillot, A. V. Zayats, F. de Fornel, *Phys. Rev. Lett.* **2001**, *86*, 1110.
[23] S. H. Chang, S. K. Gray, G. C. Schatz, *Opt. Express* **2005**, *13*, 3150.
[24] X. Zhang, Z. Li, S. Ye, S. Wu, J. Zhang, L. Cui, A. Li, T. Wang, S. Li, B. Yang, *J. Mater. Chem.* **2012**, *22*, 8903.
[25] A. G. Brolo, R. Gordon, B. Leathem, K. L. Kavanagh, *Langmuir* **2004**, *20*, 4813.
[26] A. Degiron, T. W. Ebbesen, *J. Opt. A-Pure Appl. Opt.* **2005**, *7*, S90.
[27] M. E. Stewart, N. H. Mack, V. Malyarchuk, J. A. N. T. Soares, T. Lee, S. K. Gray, R. G. Nuzzo, J. A. Rogers, *Proc. Natl. Acad. Sci. USA* **2006**, *103*, 17143.
[28] B. Auguie, W. L. Barnes, *Phys. Rev. Lett.* **2008**, *101*, 143902.
[29] H. Wu, C. J. Choi, B. T. Cunningham, *Small* **2012**, *8*, 2878.
[30] J. M. Sands, *J. Am. Soc. Nephrol.* **2007**, *18*, 670.
[31] A. Lukomska, J. Sobkowski, *J. Solid State Electrochem.* **2005**, *9*, 277.
[32] M. Moskovits, J. S. Suh, *J. Phys. Chem.* **1984**, *88*, 1293.
[33] M. R. Gartia, Z. Xu, E. Behymer, H. Nguyen, J. A. Britten, C. Larson, R. Miles, M. Bora, A. S. Chang, T. C. Bond, G. L. Liu, *Nanotechnology* **2010**, *21*, 395701.